Mitigating trajectory drift in tunnel mapping: evaluation of conventional and novel approaches applied to SLAM-based mobile mapping solution

Antonio Gualtiero Mainardi[1], Simone Marmaglio[2], Luca Perfetti[1], Giorgio Paolo Maria Vassena[1]

[1]Università degli Studi di Brescia, Dept. of Civil Engineering, Architecture, Territory,
Environment and Mathematics (DICATAM), Italy (antonio.mainardi; luca.perfetti; giorgio.vassena)@unibs.it
[2]Università degli Studi di Brescia, Dept. of Information Engineering (DII), Italy simone.marmaglio@unibs.it

Keywords: Tunnel mapping, Mobile mapping systems, Trajectory drift, SLAM, Reflectance.

Abstract

In Indoor Mobile Mapping Systems (iMMS) the trajectory estimation is implemented by the SLAM (Simultaneous Localization and Mapping) algorithm. By assuming a fixed environment surrounding the instrument, the algorithm relies on stable geometries to establish the trajectory. Drift effects represent the main source for errors and affect the trajectory estimation. These effects can be magnified in feature-deficient or degenerate environments, where the variation of geometrical elements can be minimal, as in the case of tunnels. In this context, difficult environments such as tunnels are suitable for the implementation of alternative algorithms for the trajectory estimation. Considering this kind of scenario, the contribution has the twofold objective of evaluating the results of two trajectory estimation methods, in terms of trajectory drift, with reference to an indoor SLAM-based MMS, and to establish a repeatable methodology to do so. A novel algorithm for the trajectory estimation, not just relying on geometrical SLAM algorithm, but also taking advantage of reflectance images coming from LiDAR sensors mounted on the system, is considered. The case study is a 200 m long branch of a motor-way tunnel, with a diameter of 15 m. The test is further subdivided by computing all trajectories with different constraining strategies, first without any constraints, then considering global optimisation, loop closure and static control scans, to replicate typical realistic scenarios in tunnel mapping. The results of this work highlight how the novel reflectance-aided SLAM algorithm is beneficial in terms of drift reduction in the estimated trajectories.

1. Introduction

Indoor Mobile Mapping Systems (iMMS) based on SLAM (Simultaneous Localisation And Mapping) algorithm have become a well-established solution for the rapid and detailed survey of enclosed environments. The SLAM algorithm is capable of estimating the device trajectory by computing the variation of its position in relation to a set of stable features in its surroundings (Durrant-Whyte and Bailey, 2006). Among the possible classes of systems, the one considered in this work involves the use of LiDAR and Inertial Measurement Unit (IMU) sensors, rigidly mounted on a mobile platform, allowing an operator to walk through the surveyed space while the system continuously acquires 3D point clouds and high rate inertial data. Trajectory estimation is performed by a LiDAR-Inertial Odometry (LIO) algorithm following the SLAM paradigm (Xu et al., 2022). Scan-matching step depends critically on the availability of distinctive geometric features, edges, corners and planar surfaces with varied orientations, in the surrounding environment. When such features are abundant, the trajectory can be estimated with high fidelity. In geometrically degenerate environments, however, where the scene is dominated by a poor distribution of geometrical features with repetitive or uniform shapes, the available geometric information is insufficient, resulting in an ambiguous trajectory estimate, and showcasing lack of robustness and adaptivity to environment degeneracy (Yang et al., 2026). Tunnels represent a paradigmatic example of this condition: their cylindrical cross-section provides few information along the longitudinal axis, causing the estimated trajectory to accumulate systematic errors, the so-called drift, that grows with the travelled distance.

Consequently, the drift mitigation remains one of the most complex and significant challenges in advancing this technology. In degenerate environments such as tunnels, novel algorithms able to adapt standard geometrical SLAM formulation, represent a promising direction, exploiting LiDAR reflectance images as a complementary source of information (Marmaglio et al., 2024). Feature correspondences extracted from these 2D intensity images can constrain the otherwise poorly defined trajectory estimate.

Several strategies have been proposed to counteract trajectory drift: closed loops (Hess et al., 2016) and constraints insertion, in the form of Ground Control Points (GCPs), or alternatively, in the form of georeferenced Ground Control Scans (GCSs) by terrestrial laser scanner (Marotta et al., 2022), are suggested and often necessary. Closed loops are known to facilitate the post-processing optimization of acquisition paths, and distributed constraints effectively resolve trajectory drift. However, such strategies are not often available or practical in all survey frameworks. Often in tunnel mapping, closed loops are reduced and GCPs and GCSs can be placed only at few limited locations. As shown by (Vassena, 2022), GCSs can be exploited in correspondence of the entrances of a tunnel, allowing georeferencing of the entire mobile survey. However, drift in the internal parts remains directly linked to the robustness of the SLAM algorithm and to the specific optimization method employed.

Therefore, a rigorous testing and evaluation framework is a critical component, in order to prove and validate the performances of the algorithms. In tunnels, as shown by (Yang et al., 2026), it is suggested to provide a “ground-truth” 3D model, obtained by accurate laser scanning survey, in order to establish a reference to which compare the result of the mobile mapping survey, evaluating the errors with respect to a reference trajectory.

This paper describes the methodology adopted for testing different trajectory estimation methods, with reference to a real case scenario of a tunnel mapping with a backpack indoor mobile mapping system, SLAM-based, defining a robust testing activity framework. A laser scanner survey has been conducted, to establish a 3D ground-truth point cloud of the tunnel, with centimetre-level density. Standard geometrical SLAM algorithm is compared to a novel approach taking into account reflectance images, generated by the LiDAR sensors of the system. These algorithms operate in the odometry phase, then different constraining and optimisation techniques are added, for an improvement effect in drift reduction. The comparisons among the computed trajectories, spanning all combinations of estimation algorithm and constraining method, are evaluated with respect to a “reference” trajectory, estimated exploiting the laser scanner ground-truth. The results of the comparisons are presented, with a focus on the beneficial application of the novel reflectance-based SLAM algorithm, employing established metrics for final analysis (Grupp, 2017).

1.1 Literature review

SLAM algorithm is a known research topic, present in the reference literature of robotics for more than a couple of decades so far, since the studies of (Dissanayake et al., 2001). The solution that it provides states that an autonomous vehicle is capable of starting in an unknown location and, exploiting relative observations of the surrounding environment, it is able to incrementally build a map and at the same time compute an estimate of its location. Since then, substantial development has been witnessed. In particular, the key aspects relate to the sensors utilised and the odometry algorithm exploited. The scoping review of (Gharebaghi et al., 2021), conducted over a wide range of selected articles in the field, highlights that the standard hardware core equipment is composed by LiDAR sensors and IMUs, and identifies the Extended Kalman Filter (EKF) as the most common sensors data fusion method; moreover, it recognises classical geometry-based point cloud matching, such as Iterative Closest Point (ICP) algorithm, as the most utilised.

Methods relying only on LiDAR information (LOAM – LiDAR Odometry And Mapping) can effectively work, leveraging the extraction of planar and edge features (Shan and Englot, 2018), but just for this reason they can suffer when pushing the performances in featureless environments. Levereging inertial data facilitates the retrieval of additional information for the odometry algorithm phase, for better pose estimation. Indeed, the work of (Xu and Zhang, 2021) comprises a new formula of tightly coupled iterated Kalman filter, suitable to be applied in fast navigation, mitigating drift for geometrically coherent space, but the performance in degenerate environments is unsatisfactory. Improvements in the direction of adapting the SLAM algorithm to environments with a lack of geometrical features is a common aim in the studies, leading to more advanced solutions, as the one presented by (Tuna et al., 2024), enhancing point cloud registration in geometrically uninformative conditions where ICP matching can suffer, and relying on inertial prediction in the motion direction, for example inside small tunnels. Novel approaches comprise reflectance images as a complementary source of information, improving robustness in conditions that are weak in geometry, by adding feature matching and constraining correspondences, from 2D dense reflectance images (Pfreundschuh et al., 2024). This framework needs to be extended to the case of low-resolution LiDAR reflectance images (Marmaglio et al., 2025): feature detection from LiDAR generated 2D reflectance images overcomes the problem of the possible failure of geometrical feature-based alignment, such as in tunnels or long corridors, following a standard LiDAR-Inertial Odometry (LIO) framework that fixes motion directions even with sparse correspondences. In (Wang et al., 2025), a review of the most recent advances in SLAM algorithms for degenerate environments is outlined, discussing potential future development trends.

SLAM algorithms seek for global optimisation procedures, subsequently to the odometry estimation. Closed loop detection is crucial in terms of beneficial drift compensation (Hess et al., 2016). The global optimisation problem is addressed in (Sánchez-Belenguer et al., 2020), with a sparse graph representation where local maps, featuring segmented portions of the mobile survey space, are represented by nodes connected by edges, with the aim of optimising the maps’ poses with regard to all considered matches.

Effective testing frameworks and suitable application cases have notable weight in the complete evaluation of a SLAM-based mapping solution, together with the choice of an adequate odometry for complex environments, if needed. This is the case of (Li et al., 2024), where following the description of the proposed method, a LiDAR-Inertial odometry with graph optimisation, the experimental validation is clearly presented: the validation tests are conducted in multiple subway tunnel scenarios and in an industrial park; the results of the described framework are evaluated in terms of the final estimated trajectory, compared to the identified reference one. In (Koval et al., 2022), a relative comparison between different odometry algorithms, grouped in two families (LiDAR-only and LiDAR-Inertial ones), is carried out applying the methods to an underground tunnel dataset. Also, in this case it is considered a comparison in terms only of 2D pose estimation, due to high uncertainty in the z-axis, and of final 3D point cloud.

2. Methodology

The study conducted has the dual scope of evaluating the results of two trajectory estimation methods, applied to a SLAM-based indoor Mobile Mapping, in terms of trajectory drift, and to establish a repeatable methodology to do so.

The considered trajectory estimation methods, that differ in terms of the odometry phase of the SLAM algorithm, are the following:

- **M1**, geometrical LIO-SLAM algorithm (Ceriani et al., 2015);
- **M2**, geometrical LIO-SLAM algorithm aided by LiDAR reflectance images (Marmaglio et al., 2025).

The first method, M1, is adopted in the post-processing phase of the Gexcel Heron system, a backpack SLAM-based iMMS solution that integrates multi-beam LiDAR sensors with an IMU component. Its odometry follows a standard LiDAR–Inertial scheme: a loosely coupled Error–State Kalman Filter (ESKF) fuses high-rate IMU data to produce a time-stamped trajectory used both for scan deskewing, thus compensating the

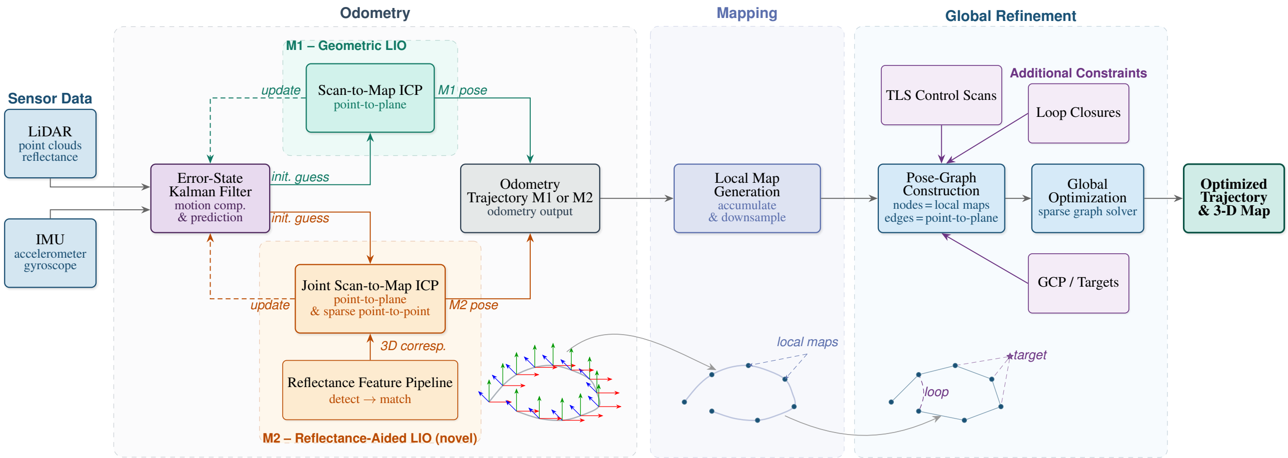

Figure 1. SLAM algorithms adopted, M1 and M2, differing for the Odometry phase.

motion of individual LiDAR returns to a common reference time, and as initial guess for the subsequent registration. An ICP step then aligns the current deskewed scan against the accumulated local map, minimising the point-to-plane error.

The alternative method, M2, retains this LIO structure, namely the same ESKF prediction, deskewing and ICP registration, but augments it with feature correspondences extracted from LiDAR reflectance images (Figure 2) (Marmaglio et al., 2025).

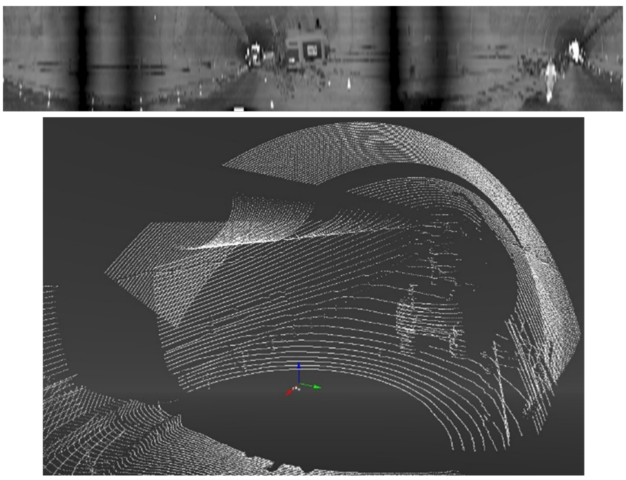

Figure 2. Reflectance image (top) and 3D scene (bottom) acquired by 32-lines multi-beam LiDAR sensors, mounted on Heron, at a specific time.

Each LiDAR sweep is projected onto the sensor’s native encoder grid to form a 2D reflectance image, whose height corresponds to the number of beams and whose width to the number of azimuth samples per revolution (Figure 2). SIFT keypoints are detected on this image and matched against a persistent tracking map of previously observed features; sub-pixel locations are then back-projected to 3D through the known scan geometry, yielding sparse 3D correspondences. The final pose is obtained by jointly minimising a weighted combination of a sparse point-to-point term from the validated reflectance correspondences and the conventional point-to-plane scan-to-map residual within the ICP framework. The sparse reflectance term supplies information along weakly observed motion directions, stabilising convergence in degenerate settings. After each optimisation cycle, the ESKF state is corrected by the ICP-derived pose update, and the reflectance tracking map is maintained by updating matched features, inserting newly detected stable keypoints and eliminating stale tracks. The reflectance-aided odometry is capable of providing reliable trajectory estimates even in degenerate environments where the standard geometrical odometry is prone to failure.

Both methods share the same global optimisation framework (Sánchez-Belenguer et al., 2020). The point cloud generated by the estimated trajectory is subdivided into local maps, rigid portions of aligned cloud accumulated over a predefined length and down-sampled. Each local map constitutes a node of a pose graph. To enrich the graph connectivity, a Kalman filter predicts the expected transformations between local maps that have not yet been associated; candidate pairs are then verified through registration, and validated matches are inserted as edges in the pose graph. The global optimisation redistributes the accumulated drift error along the entire trajectory, exploiting the redundancy of the connections. External constraints can be added to the pose graph: loop closures, when the path returns to the starting point; ground control scans, for instance from Terrestrial Laser Scanner (TLS), registered against the local maps; and known control points to anchor specific positions to the reference frame.

The schematic representation of the SLAM algorithms considered is presented in the flowchart of Figure 1.

3. Testing activity

The device considered for the discussed case study is the SLAM-based mobile mapping solution of Gexcel, namely Heron MS Twin Color (Gexcel, 2026). The Heron device is configured with two 32-lines LiDAR sensors, one placed horizontally (300 m range) and one placed 45° inclined (120 m range).

The case study is a 200 m long branch of a motor-way tunnel, with a diameter of 15 m. The acquisition started from the entrance of the tunnel, proceeding to its inner outermost part under construction, ending back at the same entrance of the tunnel (Figure 3). The test was conducted in the San Donato Tunnel, part of the expansion works of the italian A1 motorway, near Firenze.

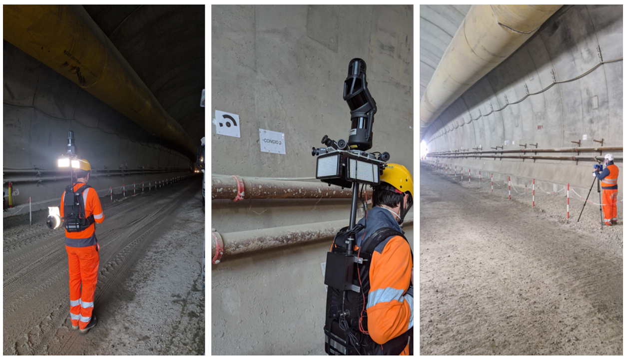

Figure 3. Survey equipment and tunnel environment.

In order to establish a robust testing framework, ground truth data is provided by a TLS survey, characterised by a centimetre-level density and estimated 2.5 cm global accuracy, and by ground control points used for the scans' registration, distributed along the tunnel, and measured via total station survey. Reference "drift free" trajectory has been estimated by exploiting all available constraints, by tracking Heron trajectories on TLS 3D point cloud (Figure 4). The procedure is conducted utilising the "tracking" odometer from the Heron device data elaboration (Sánchez et al., 2016). A reference 3D model is established, which is constituted in this case by the laser scanner point cloud of the tunnel. Subsequently, the geometrical SLAM algorithm is executed to define the ground-truth trajectory, with the ICP correspondences determined against the reference 3D model, in place of accumulated local maps.

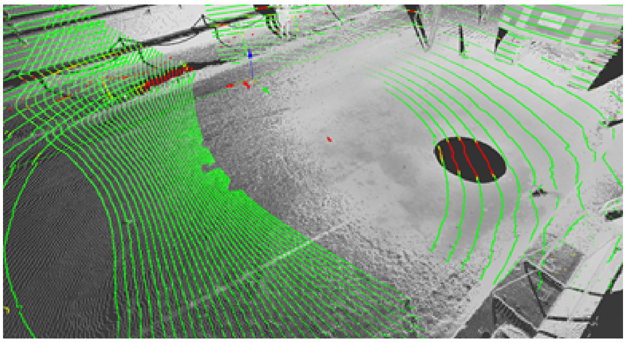

Figure 4. Tracking odometer: alignment between Heron clouds and TLS georeferenced point cloud (correspondences in green).

The test is then conducted in post-processing by computing trajectories employing the two methods, comparing the results with the reference ones. The test is further subdivided by computing all trajectories with different constraining strategies (CS):

- **CS0:** trajectory estimation depends solely on the odometry phase of the employed method, without optimisation, loop closure or any other possible constraints. Only one-way of the acquisition path is considered, from the beginning to the last position in the forward direction.
- **CS1:** as CS0, but trajectory estimation depends on the full SLAM processing, introducing global optimisation on top of previous odometry solutions. No global constraints (either GCSs or GCPs) are applied.
- **CS2:** as CS1 with added global constraints implemented at the start and at the end of the tunnel, in the form of ground control scans. This test simulates one common realistic scenario in tunnel mapping where constraints are provided at both ends.
- **CS3:** as CS1 with no global constraints; however, this time, the trajectories are computed in their entire length, considering both ways, back and forth direction, implementing the loop closure for the path returning at the beginning of the tunnel. This simulates another realistic scenario in tunnel mapping.

For cases CS0, CS1 and CS3, the corresponding point clouds have been rigidly registered with the TLS ground truth based on the first 20 metres of the tunnel, thus achieving a common reference system. CS2 is already registered in the reference coordinates system from the added global constraints. The map view of the tunnel coming from the TLS point cloud, with the indication of target and scan locations, and iMMS one with its reference path, are shown in Figure 5.

In total 8 test trajectories (T#) have been computed (Table 1).

	CS0	**CS1**	**CS2**	**CS3**
M1	T1	T2	T3	T4
M2	T5	T6	T7	T8

Table 1. Trajectories considered, combining different estimation methods and constraining strategies.

Even though the chosen tunnel scenario establishes a difficult and challenging environment for the system itself, it has to be noticed that it is characterised by some geometrical features, represented by working site equipment (see Figure 3 and Figure 5), anyway leading to interesting results for each of the eight test trajectories considered.

4. Results

The computed trajectories are evaluated through two metrics commonly adopted in SLAM benchmarking (Grupp, 2017): **Absolute Pose Error (APE)**, which calculates the pointwise difference between the estimated pose of the instrument and the reference ground truth one, providing a measure of the global accuracy; **Relative Pose Error (RPE)** over 10 m, which estimates the change in position that the device has occurred over a specified interval, with respect to the change in position of the reference trajectory, over the same interval, 10 m, capturing the local drift. Lower values of APE Root Mean Square Error (RMSE) mean higher localisation accuracy and global consistency; lower values of RPE RMSE mean better performance in local drift reduction and local stability of the odometry. The APE and RPE are referred in their traslational component.

To establish an effective and comprehensive comparison, the eight test trajectories result from combining two post-processing algorithms (M1 and M2) with four constraining conditions (CS0–CS3), as described by Table 1. To isolate the effect of the of the trajectory estimation method (M1 vs M2), each comparison pairs two trajectories that share the same constraints but differ in the estimation method: **T1 vs T5**, **T2 vs T6**, **T3 vs T7**, **T4 vs T8**.

In the following graphs (Figure 6, 7, 8, 9), the considered trajectories are plotted over a planimetric view and altimetric one, with the first pose referred as the origin and x-positive axis in the progressive tunnel direction; the tunnel slopes upward. The

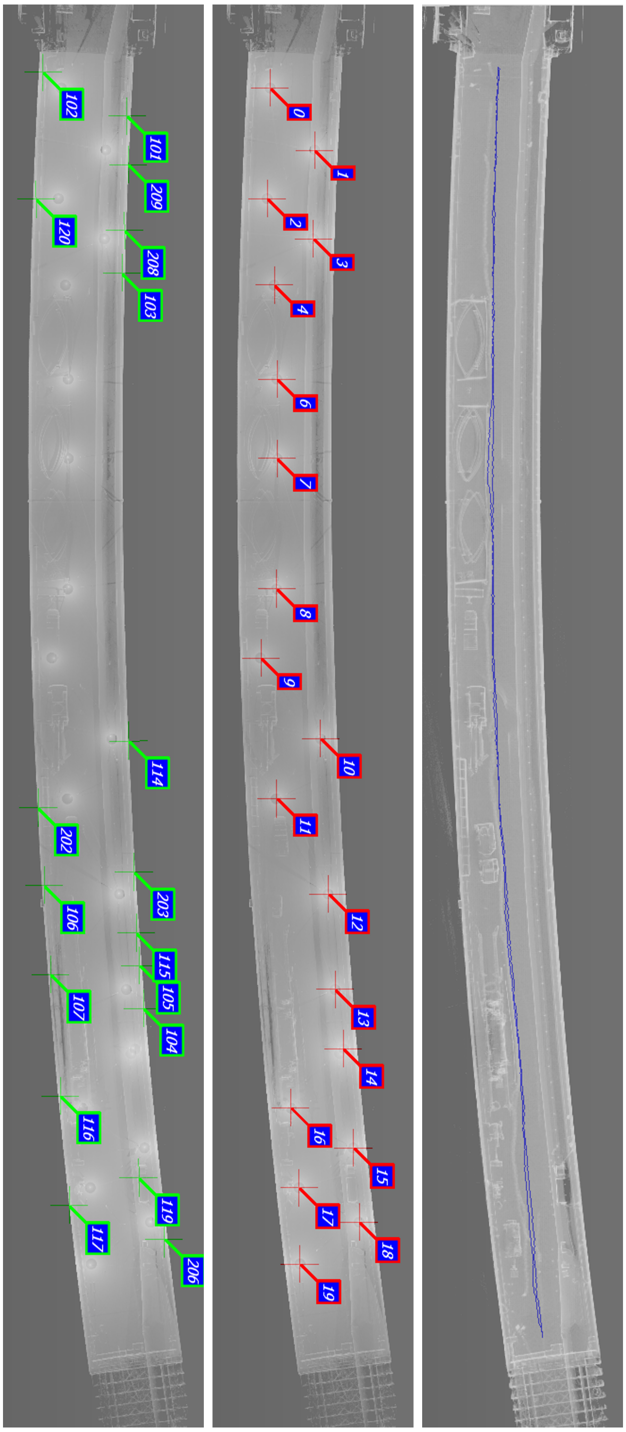

Figure 5. Tunnel Ground-Truth: map view of TLS point cloud with targets in green (left) and scanner positions in red (centre); Heron point cloud with reference trajectory in blue (right).

reference ground truth is plotted as well, and the test trajectories are coloured with respect to the reported scale, representing the APE magnitude at every pose. Over the colour scale, the maximum value of the APE for every trajectory is detailed. Moreover, a detailed zoomed view is displayed, in the corresponding portions most affected by drift effect, to facilitate the visualisation of the actual deviation of the considered trajectory against the ground-truth. Indeed, these portions more subjected to highlight the drift accumulation are either at the start or end of the tunnel, apart for the CS2 case where the drift is higher at the middle of the tunnel branch.

For every comparison, RMSE is reported in the corresponding tables (Table 2, 3, 4, 5), as statistical indicator for the analysis, for APE and for RPE over 10 m.

4.1 M1 vs M2: odometry comparison

The reflectance-aided method M2 consistently outperforms the standard geometrical odometry M1, independently from the constraining condition adopted. In terms of APE RMSE, the reduction of the error (from M1 to M2) is on a decimetre-level for CS0, CS1 and CS3, while on a centimeter-level for CS2. A similar trend holds for local accuracy: RPE RMSE improves gradually from CS0, to CS2 and CS3 that feature almost the same value. Notably, the RPE RMSE of M1 remains nearly constant across all constraint configurations (minimum value 0.048 – maximum value 0.056 m), indicating that the global refinement does not affect the local stability of trajectory estimation of the standard geometrical SLAM method.

4.2 Constraint strategy effectiveness

The four constraining strategies can be ranked by decreasing APE RMSE as: CS0 (odometry only) - CS1 (global optimisation) - CS3 (loop closure) - CS2 (control static scans), consistently for both methods. Starting from the raw odometry (CS0), global optimisation alone (CS1) reduces APE RMSE both for M1 and for M2, confirming its role in redistributing accumulated drift along the trajectory. Adding loop closure (CS3) produces a further improvement over CS1; however, as visible in the zoomed views of the graphs, drift at the outermost section of the tunnel is not fully compensated, since the return path can only partially correct errors accumulated before the turning point. The most effective strategy is CS2, where control static scans placed at both ends of the tunnel anchor the trajectory to the reference frame. This reduces APE RMSE with respect to CS0 for both methods: from 0.748 m to 0.078 m for M1 and from 0.507 m to 0.035 m for M2. In this configuration the residual drift is confined to the middle section of the tunnel, far from the constraints, reaching a maximum of approximately 0.2 m for M1, which represents the lowest APE peak among all M1 cases, and more than reduced by half for M2.

5. Conclusion and future works

The outcomes of this work highlight how the novel reflectance-aided SLAM algorithm (M2) is beneficial in terms of drift reduction in the estimated trajectories. This behaviour is consistent for all tests: from the RMSE analysis, it is highlighted a better performance of the novel SLAM algorithm, both for the APE and RPE metrics, across all constraining configurations. In the context of the presented case study, the standard geometrical SLAM (M1) proved still applicable thanks to the few geometrical features present. For what concerns the effectiveness of the constraining stategies, the global optimisation (CS1) helps in reducing the drift effect at the end of the travelled path with respect to the simple odometry (CS0); the loop closure (CS3) is not able to compensate itself the drift at the outermost section of the tunnel; the control scans applied at the edges (CS2) returns drift accumulation in the central portion, configuring as the most effective method.

Future developments will extend the application of this testing and analysis framework to other possible test sites, with

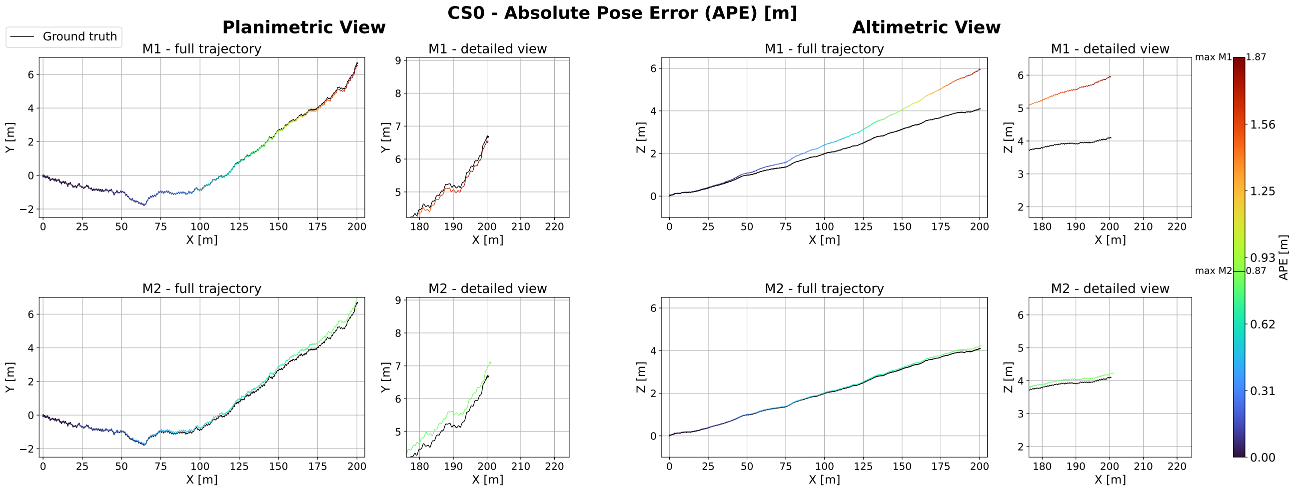

Figure 6. Comparison T1 vs T5 (CS0): trajectories coloured by APE.

	CS0	APE RMSE (m)	RPE RMSE (m)
M1	T1	0.748	0.056
M2	T5	0.507	0.048

Table 2. RMSE comparison T1 vs T5 (CS0).

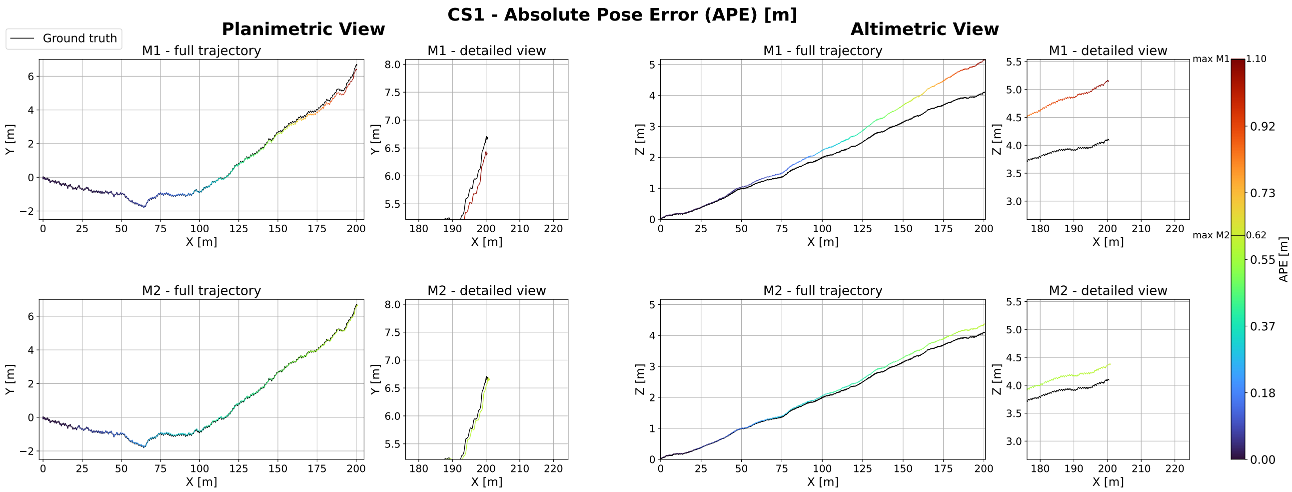

Figure 7. Comparison T2 vs T6 (CS1): trajectories coloured by APE.

	CS1	APE RMSE (m)	RPE RMSE (m)
M1	T2	0.449	0.054
M2	T6	0.347	0.035

Table 3. RMSE comparison T2 vs T6 (CS1).

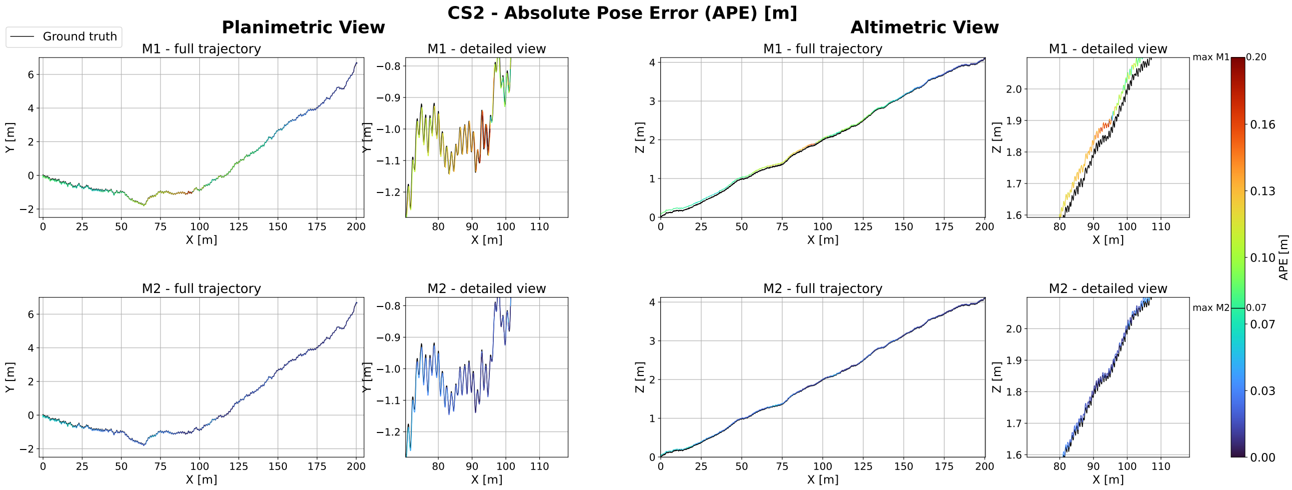

Figure 8. Comparison T3 vs T7 (CS2): trajectories coloured by APE.

	CS2	APE RMSE (m)	RPE RMSE (m)
M1	T3	0.078	0.053
M2	T7	0.035	0.024

Table 4. RMSE comparison T3 vs T7 (CS2).

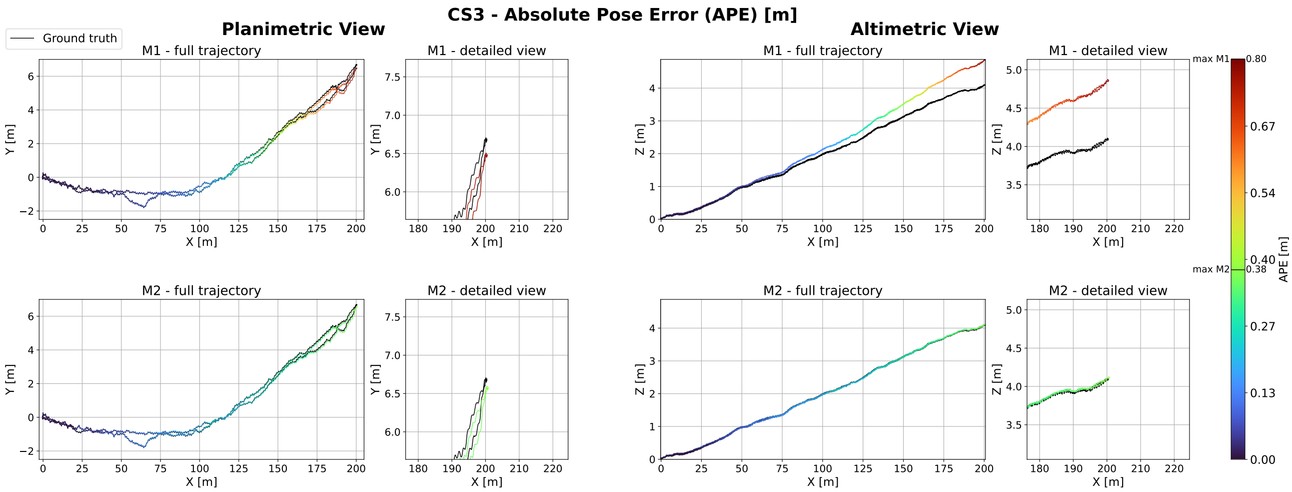

Figure 9. Comparison T4 vs T8 (CS3): trajectories coloured by APE.

	CS3	APE RMSE (m)	RPE RMSE (m)
M1	T4	0.323	0.048
M2	T8	0.208	0.026

Table 5. RMSE comparison T4 vs T8 (CS3).

even more homogeneous and degenerate environments, to challenge even more the presented SLAM algorithms, together with the expansion of the discussion involving other typologies of sensors, e.g. mobile mapping solutions based on Structure-From-Motion or Visual-SLAM algorithms, from multicamera systems, not considered in this work.

Acknowledgements

The authors would like to thank Dr. Alberto Balestrieri from Rocksoil S.p.A. and Amplia S.p.A., in particular the Construction Site Supervisor Antonio Bifano, for their support to the survey activities.

This work was funded by the European Union – Next Generation EU, Mission 4 Component 1 (CUP: D82B23003750008 and D82B23003760008).

References

Ceriani, S., Sánchez, C., Taddei, P., Wolfart, E., Sequeira, V., 2015. Pose interpolation SLAM for large maps using moving 3D sensors. *IEEE/RSJ International Conference on Intelligent Robots and Systems (IROS)*, 750–757.

Dissanayake, M., Newman, P., Clark, S., Durrant-Whyte, H., Csorba, M., 2001. A Solution to the Simultaneous Localization and Map Building (SLAM) Problem. *IEEE Transactions on Robotics and Automation*, 17(3), 229–241.

Durrant-Whyte, H., Bailey, T., 2006. Simultaneous Localization and Mapping: Part I History of the SLAM Problem. *IEEE Robotics & Automation Magazine*, 13(2), 99–110.

Gexcel, 2026. Heron MS Twin Color – Gexcel solutions for 3D surveying. `https://heron.gexcel.it/en/gexcel-solutions-for-3d-surveying/heron-portable-3d-mapping-systems/heron-ms-twin-color/`. Accessed: 26 March 2026.

Gharebaghi, A., Mostafavi, M. A., Larouche, C., Esmaeili, K., Genon, M., 2021. Precise indoor localization and mapping using mobile laser scanners: a scoping review. *Geomatica*, 75(4), 165–177.

Grupp, M., 2017. evo: Python package for the evaluation of odometry and SLAM. `https://github.com/MichaelGrupp/evo`. Accessed: 26 March 2026.

Hess, W., Kohler, D., Rapp, H., Andor, D., 2016. Real-time loop closure in 2D LiDAR SLAM. *Proceedings – IEEE International Conference on Robotics and Automation*.

Koval, A., Kanellakis, C., Nikolakopoulos, G., 2022. Evaluation of Lidar-based 3D SLAM algorithms in SubT environment. *IFAC-PapersOnLine*, 55(38), 126–131.

Li, C., Pan, W., Yuan, X., Huang, W., Yuan, C., Wang, Q., Wang, F., 2024. High-Precision Map Construction in Degraded Long Tunnel Environments of Urban Subways. *Remote Sensing*, 16(5).

Marmaglio, S., Nguyen Hoang, N., Savardi, M., Sgrenzaroli, M., Vassena, G., Signoroni, A., 2025. Degeneracy-Resilient LiDAR Odometry via Reflectance-Derived Correspondences. M. Comino Trinidad, C. Mancinelli, F. Maggioli, C. Romanengo, D. Cabiddu, D. Giorgi (eds), *Smart Tools and Applications in Graphics – Eurographics Italian Chapter Conference*, The Eurographics Association.

Marmaglio, S., Savardi, M., Hoang, N. N., Sgrenzaroli, M., Vassena, G., Signoroni, A., 2024. Leveraging LiDAR Reflectance Images for Sparse Odometry. *International Archives of the Photogrammetry, Remote Sensing and Spatial Information Sciences*, XLVIII-2/W7-2024, 73–80.

Marotta, F., Achille, C., Vassena, G., Fassi, F., 2022. Accuracy improvement of a iMMS in an urban scenario. *International Archives of the Photogrammetry, Remote Sensing and Spatial Information Sciences*, 351–358.

Pfreundschuh, P., Oleynikova, H., Cadena, C., Siegwart, R., Andersson, O., 2024. COIN-LIO: Complementary intensity-augmented LiDAR inertial odometry. *Proceedings – IEEE International Conference on Robotics and Automation*, 1730–1737.

Sánchez, C., Taddei, P., Ceriani, S., Wolfart, E., Sequeira, V., 2016. Localization and tracking in known large environments using portable real-time 3D sensors. *Computer Vision and Image Understanding*, 149, 197–208.

Sánchez-Belenguer, C., Ceriani, S., Taddei, P., Wolfart, E., Sequeira, V., 2020. Global matching of point clouds for scan registration and loop detection. *Robotics and Autonomous Systems*, 123.

Shan, T., Englot, B., 2018. LeGO-LOAM: Lightweight and ground-optimized Lidar odometry and mapping on variable terrain. *IEEE/RSJ International Conference on Intelligent Robots and Systems (IROS)*, 4758–4765.

Tuna, T., Nubert, J., Nava, Y., Khattak, S., Hutter, M., 2024. X-ICP: Localizability-Aware LiDAR Registration for Robust Localization in Extreme Environments. *IEEE Transactions on Robotics*, 40, 452–471.

Vassena, G. P. M., 2022. Outdoor and indoor mapping of a mining site by indoor mobile mapping and geo referenced ground control scans. *Proceedings of the FIG Congress 2022 – Volunteering for the Future: Geospatial Excellence for a Better Living*, International Federation of Surveyors (FIG), Warsaw, Poland. Paper no. 11590, Session TS04D.

Wang, W., Zhang, Q., Hu, Y., Gallay, M., Zheng, W., Guo, J., 2025. Recent Advances in SLAM for Degraded Environments: A Review. *IEEE Sensors Journal*, 25(15), 27898–27921.

Xu, W., Cai, Y., He, D., Lin, J., Zhang, F., 2022. FAST-LIO2: Fast Direct LiDAR-Inertial Odometry. *IEEE Transactions on Robotics*, 38(4), 2053–2073.

Xu, W., Zhang, F., 2021. FAST-LIO: A Fast, Robust LiDAR-inertial odometry package by tightly-coupled iterated Kalman filter. *IEEE Robotics and Automation Letters*, 6(2), 3317–3324.

Yang, D., Shi, W., Zhang, S., Nie, M., Wei, Y., Zhong, Q., Lu, S., Khan, A., 2026. Degeneracy-Resistant LiDAR-SLAM Algorithm Based on Geometric and Visual Features’ Fusion. *Journal of Field Robotics*, 43, 330–352.

https://doi.org/10.5194/isprs-archives-XLIX-B1-2026-25-2026